

Nanoporous silver for electrocatalysis application in alkaline fuel cells.

Daria Barsuk ^{1,2*}, Anicet Zadick ^{‡, 3,4}, Marian Chatenet ^{‡,3,4,5}, Konstantinos Georgarakis ^{1,2,6}, Nikolaos T. Panagiotopoulos ^{1,2}, Yannick Champion ^{1,2} and Alberto Moreira Jorge Jr ^{‡,1,2,3,4,7}

¹ Université Grenoble Alpes, SIMAP, F-38000 Grenoble, France

² CNRS, SIMAP, F-38000 Grenoble, France

³ Université Grenoble Alpes, LEPMI, F-38000 Grenoble, France

⁴ CNRS, LePMI, F-38000 Grenoble, France

⁵ French University Institute (IUF), Paris 75231, France

⁶ WPI-AIMR, Tohoku University, Sendai 980-8577, Japan

⁷ Federal University of São Carlos, DEMa, São Paulo 13565-905, Brazil.

KEYWORDS: Nanoporous, silver alloys, dealloying, ammonia-borane, fuel cell, electrooxidation.

ABSTRACT: Self-supporting porous silver foils with an average pore size less than 100 nm were produced from a crystalline silver-based ternary alloy as a precursor by removing second phases present in the silver matrix. The final Ag-based porous foil shows good mechanical properties when comparing to its previous amorphous analogues. Its activity for direct electrochemical oxidation of ammonia-borane (AB), a fuel of interest for direct liquid fuel cells, has been investigated in alkaline media. The material exhibits promising electrochemical properties in long-term operation; indeed, material composition and nanostructure remain similar after 15 000 cyclic-voltammeteries between -0.3 and 0.5 V vs. RHE in a 0.1 M NaOH + 5 mM AB solution thermostated at 25 °C. Nanoporous materials, and in particular nanoporous silver, can therefore represent a relevant choice as anode in direct ammonia-borane fuel cell.

1. INTRODUCTION

With the crescent global warming due to greenhouse gas emissions, the political and environmental climates are increasingly affected, and the demand for alternative fuels becomes unquestionably clear. Hydrogen arises as a clean-energy option, generating only water after burning or electrooxidation. However, current technologies for hydrogen production, storage and transportation still require several shortcomings to be solved, for instance, green origin of the mother fuel (at present H₂ is processed from fossil fuel for more than 95% of its production) safety, energy-density, efficiency and cost.

Chemical hydrogen storage, in which hydrogen covalently bonded to molecules is released in gaseous form through (catalyzed) chemical reactions, offers a promising future for hydrogen storage and distribution. Considering the US Department of Energy target for the entire system weight (9.0 wt% H),^[1,2] the compound ammonia-borane (H₃NBH₃, AB), with a molecular weight of 30.9 g/mol and an inherent capacity of 19.6 wt % H₂, is an obvious prime candidate as hydrogen storage compound. Solution and solid-state thermal dehydrogenation,^[3-5] as well as acid-catalyzed dehydrocoupling,^[6] have been reported for hydrogen production from amine-boranes. Transition-metal-catalyzed dehydrogenation reactions have only recently been described in the literature.^[7-11] Precious noble metal catalysts (platinum-group metals - PGM) are active for AB dehydrocoupling at room temperature with catalyst loadings as low as 0.5 mol %.^[5]

Nevertheless, the above methodologies still suffer some drawbacks, which limit their utilization. PGMs are too

expensive and poorly available. As such, PGM nanoparticles are usually supported on carbon black, which are of difficult manipulation and are not so good electron conductors. Finally, the degradation of these catalyst materials is another issue: noble metal nanoparticles were recently found highly instable in strong alkaline solutions.^[12-14]

Ammonia-borane is chemically stable in an alkaline medium ^[15] and its direct oxidation in Alkaline Fuel Cells (AFCs) can solve many of those issues. Indeed, AFCs present many advantages: for instance, the kinetics of many complex reactions is non-negligibly improved in an alkaline medium, and several metals (or metal oxides) are both active and stable in alkaline media (spreading the possibilities for material candidates to be used as electrodes).^[16]

More importantly, by using an appropriate catalyst, the direct electrooxidation of ammonia-borane can initiate below the hydrogen oxidation potential ^[17](< 0 V vs. RHE, and as low as -0.3 V vs. RHE ^[18]), enhancing the energy efficiency of a Direct Ammonia-Borane Fuel Cell (DABFC) versus a hydrogen fuel cell fed after catalytic decomposition of borane fuels (in other words, the same number of electrons can be generated, but at much lower electrode potential). As such, the DABFC technology represents an interesting solution, in principle capable both of storing chemical energy and releasing it on demand with a reasonable efficiency and power density. Strong efforts have been realized to develop and improve AB oxidation catalysts ^[15,19-21] and use them in (hope-fully efficient and economically viable) DABFC.^[18]

Given that both Zadick et al. [12,13] and Olu et al. [18] have brought evidences of the huge instability of platinum, and to a lesser extent of palladium nanoparticles supported on high surface area carbon in alkaline medium, the present research aims to develop cheaper and more abundant alternative catalysts for the electrochemical oxidation amine-boranes and their valorization in DABFC. In doing so, attention is paid to the catalyst durability and stability of performance. Silver in the form of nanoparticles, agglomerates, clusters and porous substances has already been widely used as catalysts in fuel cells and electrochemical actuators, [22–25] in particular recently for the electrooxidation of borohydride compounds. [26–30] In that regards, nanoporous silver materials was evaluated as a potential anode catalyst for the DABFC.

There are many ways to elaborate metal-based porous catalysts. For instance, dissolution, a simple but powerful elaboration strategy, is commonly used to obtain nanoporous metallic systems. As a result of dissolution, less-noble elements are selectively leached from the mother alloy, driving a reorganization of nobler elements of the alloy-electrolyte interface into a 3-dimensional pattern. [31,32] This is commonly constituted by the noblest element, but it can also have a multi-elemental composition. [33–36] Crystalline alloys preserve their original microstructure after leaching: in other words, each grain becomes a crystal surrounded by a porous structure. [37]

Nanoporous metals find their application as sensors, [38,39] catalysts, [23,35,36,40–42] actuators, [43]–[44] SERS substrates, [42,45,46] and often combine advantageous structural properties with bactericidal and biocompatible ones. [47–49] Due to their very high specific surface area, nanoporous metals may present excellent catalytic properties for a series of important heterogeneous reactions, because of interconnected ligaments and 3D channels that may allow free transport of medium molecules and electrons. [50–52]

Since the development of the field of nanoporous metals, a great number of works has been dedicated to the design of noble metal-based nanoporous architected structures, among which silver plays an important role. [46,53–56] Among others, nanoporous silver (NPS) was obtained in the group of De Hosson by dealloying Al from the amorphous Ag-Al precursor alloy. [57] Another interesting “clean” method of its fabrication was recently suggested by the group of T. Zhang when amorphous Ag-Ca foils were simply immersed in water to remove calcium atoms. [55]

In the previous work by M. Zhang et al [56] was reported the fabrication of a porous silver material with a sub-micron pore size. The precursor of the given work was an amorphous $\text{Ag}_{38.75}\text{Cu}_{38.75}\text{Si}_{22.5}$ alloy that was exposed to an appropriate etching condition in order to eliminate Cu and Si atoms, leaving a single Ag porous carcass. Homogeneous distribution of elements in the amorphous state is a key to obtain the fine ultimate porous architecture upon reorganization of Ag atoms while etching; on the contrary, when in crystalline precursors are used, the final characteristic features are determined by the phases present in the ingot. [24] However, in spite of the finely archi-

tected structure, the bulk material produced from the amorphous precursor [56] did not possess sufficient mechanical integrity and robustness to allow any further experiments revealing its advantages, particularly in the field of catalysis where good failure resistance is required.

The general aim of our work is firstly to approach the structural composition of previously elaborated NPS foils so as to enhance their mechanical characteristics. In the present paper, we make a step beyond and characterize a porous silver material from an electrochemical viewpoint, in particular versus the direct electrooxidation reaction of ammonia-borane in an alkaline medium, a model reaction of interest towards the development of direct alkaline fuel cells. Besides, the stability of this material is also investigated in accelerated stress-test operation.

2. EXPERIMENTAL SECTION

2.1. Materials' preparation and characterization

A set of Ag-based polycrystalline alloys of composition $\text{Ag}_{38.75}\text{Cu}_{38.75}\text{Si}_{22.5}$ were prepared by arc melting of pure Ag, Cu and Si (99,99% purity, Alfa Aesar) in helium atmosphere. To homogenize the alloy, minimum 5 additional melting steps were made before the rapid solidification casting of the material on the copper wheel. Foils with thicknesses ranging between 20 and 60 μm were produced by varying the rotating speed of the copper wheel. After analyzing X-ray diffraction (XRD) results and preliminary chemical treatment tests of the obtained samples, the 20 μm thick foils showed finer porous architecture and were chosen for further careful characterization and ammonia-borane electrooxidation tests.

The XRD patterns of as-spun and dealloyed components were obtained using a PANalytical X'Pert Pro MRD instrument with a copper ($K\alpha$) radiation ($0.051^\circ/\text{step}$, in variable mode).

The microstructures and chemical compositions of the ribbons were observed using a high-resolution ZEISS Ultra 55 scanning electron microscope equipped with a field emission gun (FEG-SEM) and energy-dispersive X-ray analyzer (EDS).

To analyze the pore size of the as-dealloyed ribbons an imaging tool ImageJ [58] was used. Brunauer-Emmett-Teller (BET) surface area was measured by Nitrogen adsorption/desorption experiments carried out at 77 K using a Micromeritics A2020 instrument. Dealloying of the as-cast ribbons was performed at the ambient conditions using a few chemical etchants including the one reported in [56] – 13.4 wt% (2.12 M) of HNO_3 , and another solution of 0.67 M of HNO_3 and 0.64 M of HF in deionized water. The intensity of magnetic stirring while etching was 250 rpm, the etching time was chosen in the way to leave the desirable thickness of the middle bulk non-etched layer.

2.2. Electrochemical characterization

For the electrochemical experiments, silver materials were carefully cut and placed on a glassy carbon

electrode to be used as working electrode; the geometrical surface of silver materials in contact with the electrolyte was 0.048 cm^2 . The counter-electrode was a carbon plate, and the reference electrode was a mercury/mercury oxide electrode (Hg/HgO) filled with 0.1 M NaOH solution; to ease the comparison with the literature, all potential values are given versus the Reversible Hydrogen Electrode scale (RHE).

Electrolytes were freshly prepared with NaOH monohydrated provided from Merck (Suprapur), ammonia-borane provided from Sigma-Aldrich (complex, 97%) and MQ-grade water ($18.2 \text{ M}\Omega \text{ cm}$, $<3 \text{ ppb}$ total organic carbon, Elix + Milli-Q Gradient, Millipore). The electrochemical set-up was thermostated at 25°C .

3. RESULTS AND DISCUSSIONS

3.1. Production and characterization of nanoporous silver

The architectural design of nanoporous silver in this work was based on the composition and structure previously elaborated by our group.[56] However, the aim was to improve the mechanical stability, and to produce self-supporting electrodes that enable their use in electrocatalysis. Firstly, $\text{Ag}_{38.75}\text{Cu}_{38.75}\text{Si}_{22.5}$ alloys were produced using the planar flow casting technique aiming to obtain wider and thicker amorphous ribbons. The low glass forming ability of this system has disallowed the production of samples with amorphous structure and desired properties. Then, sets of crystalline ribbons of composition $\text{Ag}_{38.75}\text{Cu}_{38.75}\text{Si}_{22.5}$ were obtained by melt spinning in helium atmosphere with rotation speeds of $14\text{--}28 \text{ m/s}$. The foils had widths of $\sim 2 \text{ mm}$. According to the rotation speed, their thickness varied within the range of 20 to $60 \mu\text{m}$. The sample with the thickness of $20 \mu\text{m}$ was chosen for further chemical treatment. Its X-ray diffraction (XRD) pattern (Figure 1) confirmed that the majority of the samples was composed by the crystalline face-centered cubic silver and the hexagonal $\eta \text{ Cu}_3\text{Si}$ phase

Figure 2 represents a SEM micrograph obtained after 10 minutes of etching of the as cast selected sample in 3.32 M of HNO_3 solution. It reveals an irregular morphology and difficulties for solution penetration, without a well-defined tridimensional porous structure. Compositional analysis based on energy dispersive X-ray spectroscopy (EDS) confirmed that the atomic concentration of the residual Si atoms was $\sim 19 \text{ at}\%$.

Another etching solution: a mixture of 0.67 M of HNO_3 and 0.64 M of HF, was tested for as spun ribbons in order to accelerate the dissolution of the Si atoms. The etching time of 45 minutes was selected as an optimal time to generate a fairly regular porous structure (Figures 3 a-b).

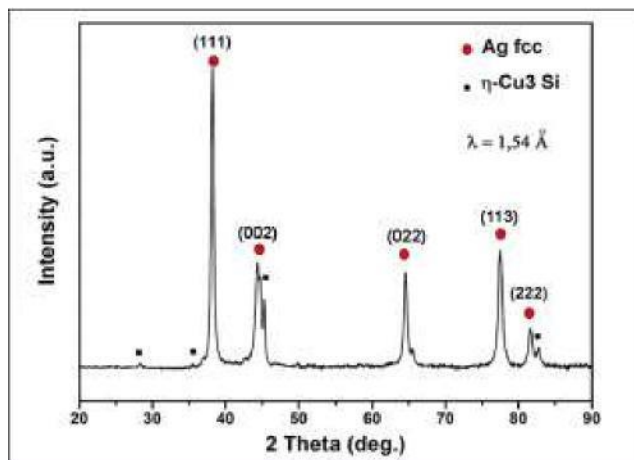


Figure 1. XRD pattern of as cast $\text{Ag}_{38.75}\text{Cu}_{38.75}\text{Si}_{22.5}$ ribbon.

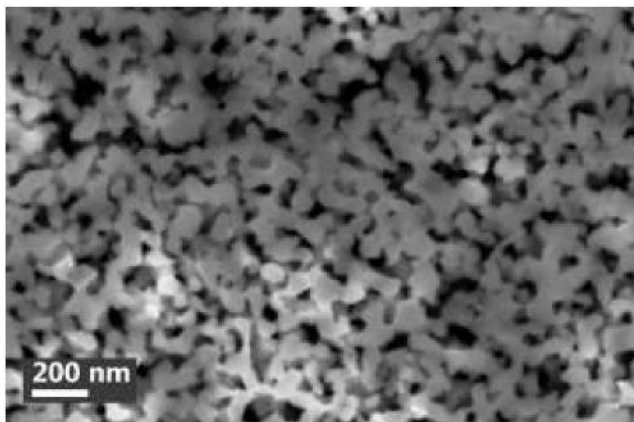


Figure 2. SEM image of a porous Ag-based pattern after dealloying in nitric acid solution for 10 min.

A 3D-architecture was readily produced, leaving in the center a thin carcass layer of few microns thick (Figure 3c). This carcass will play a load-bearing function of the material. After etching, XRD analysis reveals only the presence of fcc-Ag (Figure 3d).

Figure 4a confirms this finding. The chemical analysis, performed on the cross-section of ribbons before and after etching, reveals that all the copper and silicon have been removed after etching (although traces may subsist, below the detection limit of the EDS analyses). After longer etching time, Ag crystallites start agglomerating and the porous network of the crystalline precursor collapses, leaving a sponge-like structure, as presented in Figure 4b.

The higher chemical stability of Ag in the given acid media, in contrast to copper and silicon, is supported by the difference between standard electrode potentials of the pure elements, which, in fact, globally reflects the material nature: $e_{\text{Ag}} = 0.799 \text{ V} > e_{\text{Cu}} = 0.337 \text{ V} > e_{\text{Si}} = -0.91 \text{ V}$. All the values here are given according to the hydrogen scale.[59]

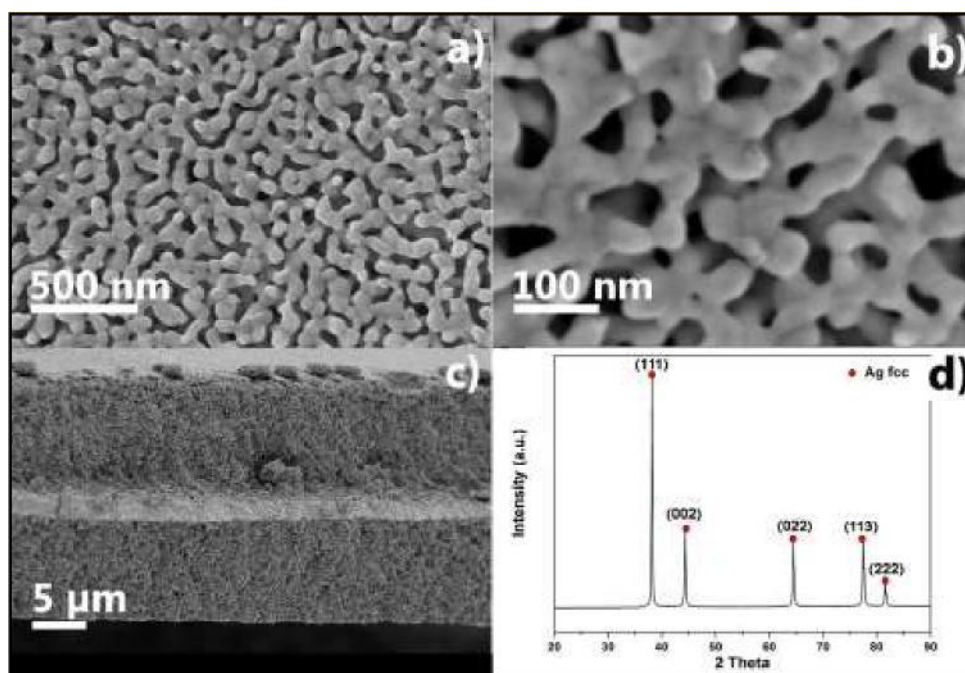


Figure 3. a), b) Surface view of the final porous microstructure c) Cross section view of the dealloyed ribbon with a bulk non-etched carcass layer in the middle d) XRD pattern of as-dealloyed $\text{Ag}_{38.75}\text{Cu}_{38.75}\text{Si}_{22.5}$ ribbons.

By using image analysis, the average surface pore size is calculated as ~ 98 nm. The ligaments on the surface are very similar. Their direct dimensions measurements gave the average values of ~ 80 nm and ~ 250 nm for the width and length, respectively. The quality of such geometry appears to be inferior to the one obtained using an amorphous precursor of the same composition, which is characterized by regular pore size distribution and its smaller dimensions (Figure 5). Nevertheless, porosity was analyzed by the method of Brunauer, Emmet and Teller (BET).[60] Figure 6 presents the pore size distribution of such measurement. Almost 76 % in volume of pores falls in a wide range of size distribution, between 4 to 102 nm. As one can observe, the size of the pores tangibly decreases going towards the bulk. It is expected that greater pore size will prevail on the surface (which is consistent with the image analyses above) while the finest ones in the interior of the foil, thus creating a sort of porosity gradient from the bulk (interior) to the surface (exterior) of the ribbons.

In the above sense, the obtained architecture, which usually consists of interconnected networks, appears to be the ideal for catalyst materials. In other words, the smaller pores will have the largest surface area. They will be the responsible for most of the catalytic reactions, while the larger pores will facilitate both fuel access and gas release, a strategy already used with success by the group of At-anassov for the alkaline oxidation of several fuels.[50– 52,61–65] The total surface area calculated by BET is ~ 5 m^2/g . The average pore size of 36 nm was calculated by the Barrett-Joyner-Halenda (BJH) method, which uses the Kelvin Model for pore-filling, being applicable to the present type of material.[66] Eventually, the final material presented a huge total surface

area, and better integrity makes it possible to apply this material as a self-supporting electrode, allowing to perform electroactivity measurements in the scope of the present work. The corresponding data are discussed below.

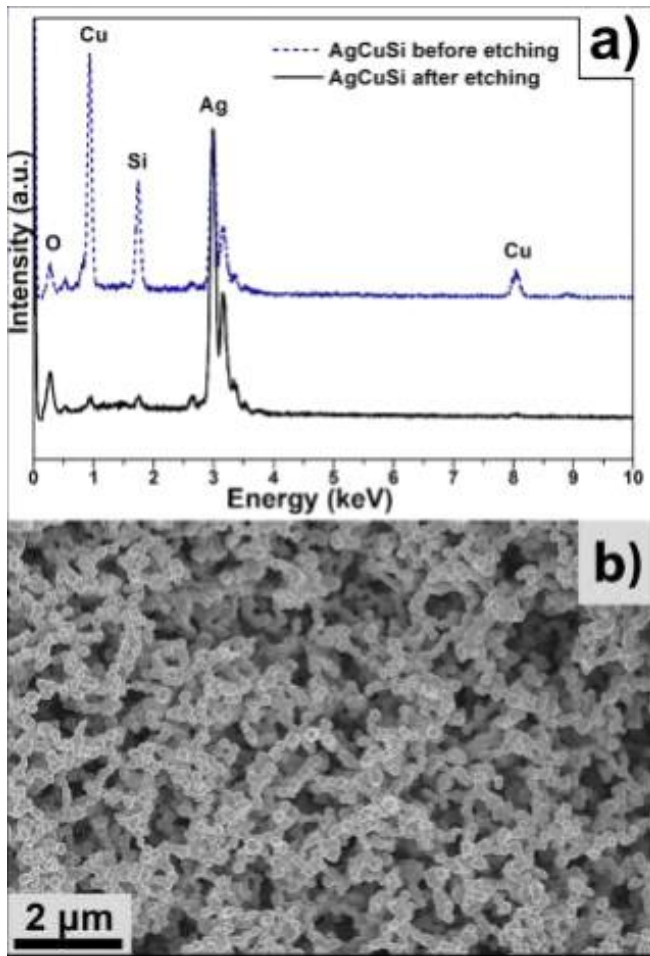


Figure 4. a) EDS spectra obtained on of the cross section of the foil before and after dealloying in the solution of mixed nitric and hydrofluoric acids for 45 min. b) SEM image of a sponge-like silver based structure after 2 hours etching

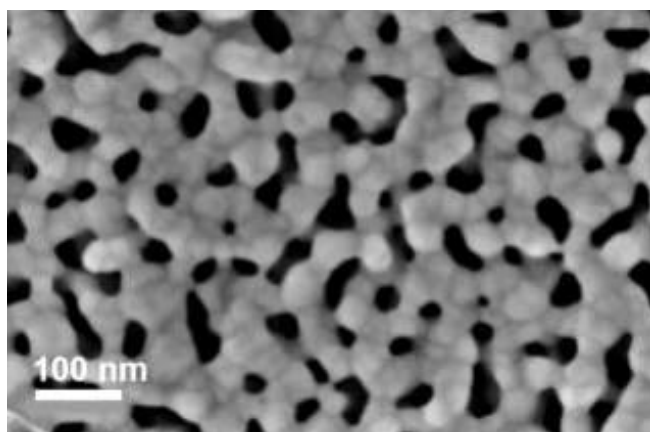


Figure 5. Nanoporous silver, obtained from the amorphous $\text{Ag}_{38.75}\text{Cu}_{38.75}\text{Si}_{22.5}$ precursor.[56]

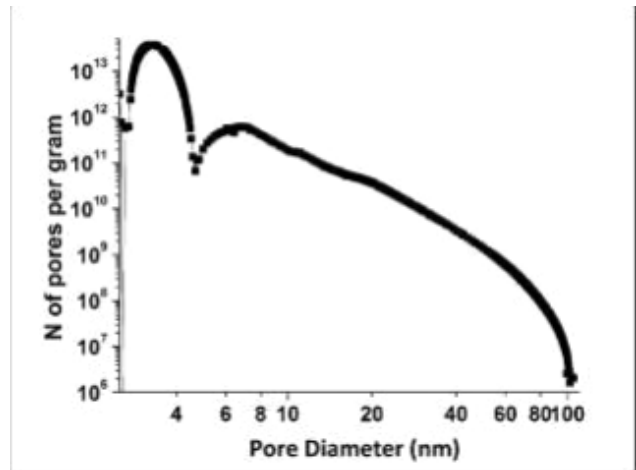


Fig.6 Pore size distribution measured by BET.

3.2. Electrochemical test

The electrocatalytic performance of porous silver for the direct electrooxidation of ammonia borane in an alkaline medium is presented on Figure 7. The cyclic voltamperogram of the nanoporous Ag substrate in the supporting electrolyte (0.1 M NaOH) reveals the nature of the silver surface (black curve – this voltamperogram being unaffected by the revolution rate of the rotating disk electrode). The large anodic peak centered at ca. $E = 0.41$ V results from the formation of surface silver oxides. The formation of copper oxides from residual copper coming from the bulk layer in the middle of the sample (Figure 3c) may also occur in this anodic peak. During the subsequent negative scan, the cathodic reduction of silver oxide proceeds, producing a peak centered at ca. 0.36 V. It is also likely that copper oxides are reduced in this potential domain, as attested by the electrochemical equilibrium between Cu and Cu_2O , expected to thermodynamically proceed around $E = 0.471$ VS. RHE.[67] Further discussion regarding copper will be given in the following sections.

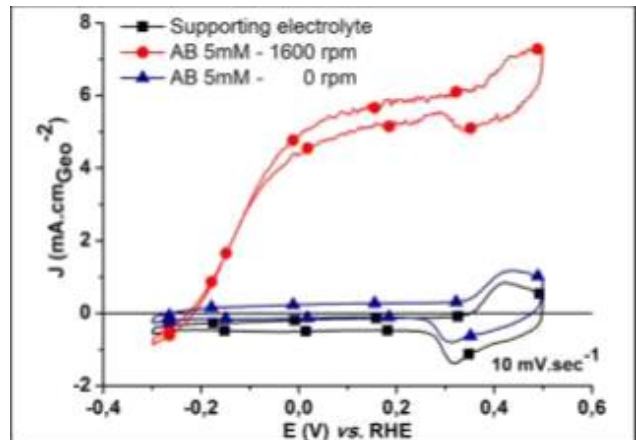


Figure 7. Electrocatalytic performances of nanoporous silver for direct ammonia borane electrooxidation in 0.1 M NaOH (black) and 0.1 M NaOH + 5 mM AB (blue), at $w = 0$ and $w = 1600$ rpm (red). All experiments were performed at 25°C .

The addition of 5 mM of ammonia-borane into the solution noticeably modifies the shape of the cyclic voltammogram, and the obtained shape is strongly depending on the revolution rate of the rotating disk electrode. An oxidation current is observed on the whole potential domain investigated, its magnitude being much larger under diffusion convection regime ($\omega = 1600$ rpm, upper red curve in Figure 7, round symbols) than on a static electrode ($\omega = 0$ rpm, lower red curve in Figure 7, triangle symbols). The reaction begins at a very low potential value, much lower than the hydrogen oxidation potential. Indeed, the onset for the electrooxidation of ammonia-borane is about $E = -0.3$ V vs. RHE (300 mV below the oxidation of hydrogen in a hydrogen-fed fuel cell), which is of utmost interest for energy production in direct alkaline fuel cells. The kinetic is relatively fast according to the steep slope of the wave in the region up to 0.3 V vs. RHE. Then, the AB oxidation current density reaches a stable maximum value of 6,44 mA/cm² at about 0.3 V vs. RHE. These values are better than the ones observed for NPGold in 1 M NaOH containing higher concentration in ammonia-borane (20 mM) or NaBH₄: the onset potential for the electrooxidation of NaBH₄ : on NPGold was at best as high as ca 0.1 V vs. RHE [68], while that of AB electrooxidation could reach -0.2 V vs. RHE [19], *i.e.* was at best shifted positive by 0.1 V compared to the best results with the present nanoporous Ag.

Comparing the voltamperograms after addition of 5 mM of ammonia-borane ($\omega = 0$ rpm and $\omega = 1600$ rpm) in Figure 7, one clearly sees that the reaction is controlled by mass-transport. Figure 8.a further presents the effect of the rotation rate of the electrode on the electrocatalytic performance measured at $E = 0$ V vs. RHE (*i.e.* at an electrode potential where a classical H₂-oxidation electrode would not release any quantitative current, which demonstrates the interest of AB oxidation at NPS electrodes); the faster the electrode is rotated, the higher the current density value, in agreement with the Levich theory. This dependency on the mass-transport means that the NPS electrode is indeed a good AB oxidation catalyst (it is not limited by charge-transfer kinetics, even at a potential as low as 0 V vs. RHE and at 25 °C); on the contrary, it implies that the fluidics of the DABFC systems should be considered with care (but this is beyond the focus of the present contribution). Besides the normal “Levich behavior”, the design of our rotating electrode can account to some extent to the mass-transport effect observed. The NPS is inserted at a position about 2 mm deep in a cylindrical shape gap, overall limiting the access of “fresh fuel” to the NPS surface. In addition, stagnant AB electrolytes are prone to severe heterogeneous hydrolysis at the NPS electrode; indeed, we observed hydrogen gas

bubbles being stacked in the gap. Besides consuming the AB fuel and only being prone to be oxidized above $E = 0$ V vs. RHE, the presence of such H₂ bubbles may interrupt the contact between the NPS catalyst and the AB solution, resulting in lower oxidation current. In any of these cases, the performance of the NPS electrode is improved by increasing the revolution rate of the rotating disk electrode: doing so firstly enables the access of “fresh AB” fuel and secondly favors the removal of hydrogen gas bubbles. It has to be noted that, whatever the steps of revolution rates, the current density increases/decreases rapidly as soon as the rotation of the working electrode is changed, denoting for the absence of poisoning/deactivation of the NPS electrode in the course of the AB oxidation. Besides, the two sequences measured at $\omega = 1600$ rpm demonstrate that the NPS proceeds without any quantitative loss in activity versus time (within the time frame of the present experiments).

The stability of the oxidation reaction current was further analyzed; samples were held at $E = 0$ V vs. RHE (Figure 8.b) for 10 minutes. The NPS electrode presents a stable short-term activity for AB oxidation; this is promptly observable by the very small loss of activity during the period of tests, represented by the small decrease in the oxidation current density and rules out any severe effect of poisoning of the Ag surface by reaction intermediates, as shown for the electrooxidation of NaBH₄ at Pt surfaces [17,69,70].

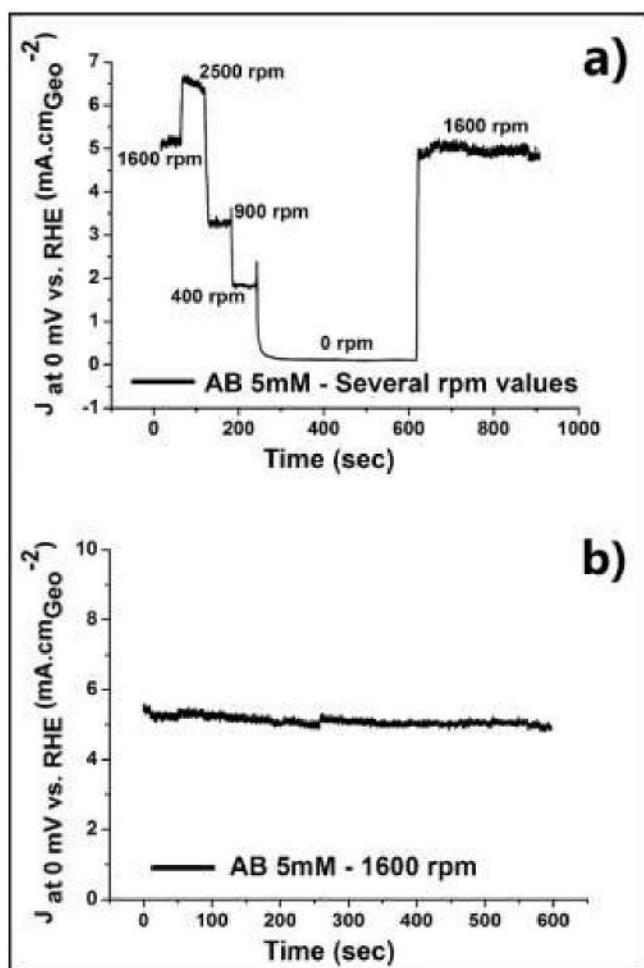


Figure 8: a) Effect of the electrode's rotation speed and b) Signal stability, for direct Ammonia Borane electrooxidation. All performed in 0.1 M NaOH + 5 mM AB, at 0 V vs. RHE and 25 °C.

In addition, the structural stability of the nanoporous silver and its AB oxidation activity have been investigated for long-term operation (the accelerated stress test, AST, consisted of up to 15000 000 voltamperometric cycles between -0.3 and 0.5 V vs. RHE at 100 mV/s) in the same electrolyte (0.1 M NaOH + 5 mM AB, at 25 °C). Cyclic voltammograms and representative SEM images are given in Figure 9 and Figure 10, respectively. In Figure 9, one can clearly see that the behavior of nanoporous silver remains similar even after 15000 cycles; only minor diminution of the anodic current density values can be observed by cycling in the electrolyte: it is a consequence of the ammonia-borane rarefaction in the electrolyte due to its progressive consumption at the working electrode. In spite of this globally decreasing anodic current contribution from AB oxidation, there are no major changes in the equilibrium between the silver/silver oxides (and possibly copper/copper oxides) peaks and for the capacitive current values (in particular, the silver (and copper) oxides reduction peak at ca. 0.3 V vs. RHE in the negative

sweep, which is not biased by the AB oxidation current is literally unchanged from the 1st to 15,000th cycle of the AST); this indicates that neither metal dissolution, nor active surface area loss, nor structural changes of the silver nanoporous do happen during the cycling. As one can observe in Figure 10, there are neither significant changes in the morphology of the ligaments or pores of the NPS material after this accelerated stress test. The conjunction of these two results suggests the chemical and electrochemical stabilities of the catalyst in long-term operation. Nevertheless, occasional agglomerates have appeared on the electrode surface. EDS analyses demonstrate that they are rich in copper; such copper-rich islands were not observed for the fresh electrode. Copper has therefore migrated from the bulk to the surface of the sample in the course of the aging test. This, in fact confirms that the oxidation/reduction peaks observed around 0.4 V vs. RHE in Figure 7 are related both to silver (major-ly) and copper (minorly). Copper necessarily comes from the bulk layer in the middle of the sample (Figure 3c) where the alloying elements (Cu and Si) remained unaltered after the leaching procedure.

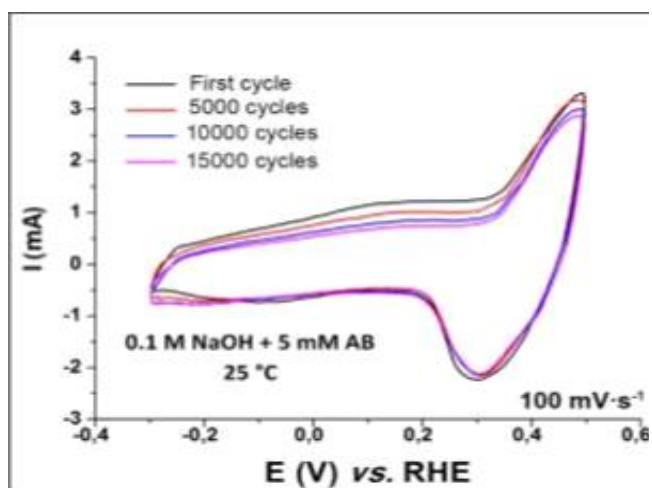


Figure 9. Cyclic voltammeteries of NPS material after 0, 5000, 10 000 and 15 000 cycles in 0.1 M NaOH + 5 mM AB at 100 mV/s and 25°C.

However, such changes are overall very minor and the porosity of the NPS sample remains essentially unaltered even after 15,000 cycles; this stability is already larger than what has been observed for noble electrocatalysts of platinum nanoparticles supported on high surface area carbon as previously reported in.[12,13]

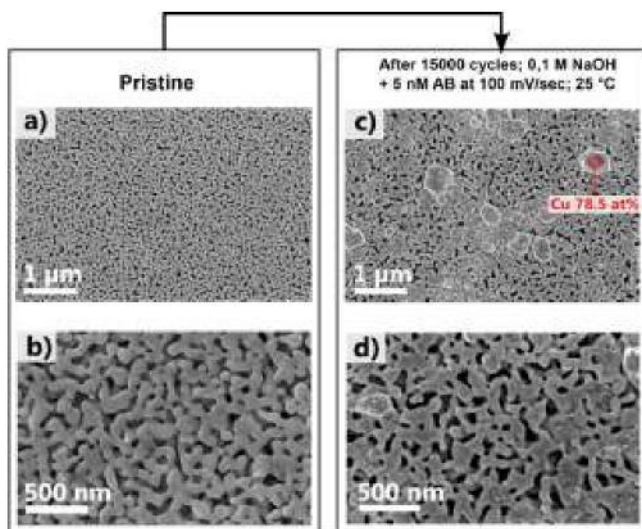


Figure 10. SEM images of porous silver before (a.-b.) and after (c.-d.) 15,000 Cyclic voltammeteries performed between -0.3 and 0.5 V vs. RHE at 100 mV/s in 0.1 M NaOH + 5 mM AB, at 25 °C.

In addition, such dissolution (from the bulk of the NPS sample) and precipitation (at its surface) of Cu-rich agglomerates is another indication that the whole NPS sample is accessible to reactants, owing to its porous architecture. If such diffusion of Cu atoms/ions from the bulk to the surface of the NPS proceeds, it is likely that AB and its oxidation products can do as well, in agreement with the good electrochemical performances monitored above. To be more specific, the porous architecture of the NPS, formed by the conjunction of very small channels in diameter with large surface area in the middle, channels which enlarge in diameter towards the surface, facilitate the intrusion of the AB-containing liquid solution and the release of the hydrogen bubbles possibly formed from heterogeneous hydrolysis and other AB oxidation products. These textural properties coupled to the intrinsic ability of Ag to promote AB oxidation reaction enable to understand the steep wave monitored on Figure 7, indicating large overall AB oxidation activity.

From these results, NPS seems both very active and durable for the direct electrooxidation of ammonia-borane in alkaline medium. In addition, the residuals of the secondary η -phase in the final porous structure do not perturbate the oxidation process of AB, which means that material does not require any remarkable purity level in order to be exploited in real conditions.

4. SUMMARY AND CONCLUSIONS

Foils of nanoporous silver were synthesized from a crystalline $\text{Ag}_{38.75}\text{Cu}_{38.75}\text{Si}_{22.5}$ precursor by free corrosion in an acid solution. Further, by controlling the etching parameters, nanoporous silver foils were designed to have a thick nanoporous layer and a bulk thin layer of the nominal composition, which contributed to their mechanical stability a clear advantageous for application in self-supporting catalysts. It is for the first time that NPS foils

have been successfully tested as an active and stable material for direct ammonia-borane electrooxidation in an alkaline medium, which was not possible for its nanoporous analogue, produced from amorphous precursor (the material could not self-stand and could not be handled to prepare electrodes). Moreover, the material appeared to be competitive to nanoporous gold substrate, and economically is more advantageous, owing to the smaller cost and larger availability of silver compared to gold. The architecture of the present porous material follows the design of the most modern current catalysts. These are formed by very small pore channels, in which the reaction will occur due to the extremely active large surface area and increased pore channel diameters going towards to the surface, which favors both liquid and gas transportation.

The results presented in this work are inspiring and they open optimistic prospects for nanoporous silver and likely for other cheaper transition metal-based materials for their direct application in fuel cells as a lower-cost integral/ergonomic alternative for platinum nanoparticles supported on high surface area carbon materials.

ASSOCIATED CONTENT

AUTHOR INFORMATION

Supporting Information

The supporting information includes EDS data on the material, dealloyed for 10 minutes in 13.4 wt% HNO_3 solution. Optical images of as-cast and dealloyed material, and images exhibiting structure evolution with the dealloying time.

Corresponding Author

* [E-mail: daria.barsuk@simap.grenoble-inp.fr](mailto:daria.barsuk@simap.grenoble-inp.fr)

Author Contributions

All authors have given approval to the final version of the manuscript. ‡ These authors contributed equally.

Funding Sources

This work was partially supported by the European ITN Network project “VitriMetTech” (grant No. FP7-PEOPLE-2013-ITN-607080 in frames of Marie Skłodowska-Curie actions program; and by the Rhône-Alpes Academic Research Community l’ARC Energies (grant No. 13-009671-01).

ACKNOWLEDGMENT

A. Zadick acknowledges Centre of Excellence of Multifunctional Architected Materials “CEMAM”, project No. AN-10-LABX-44-01. M. Chatenet thanks the French IUF for its support. A. M. Jorge Junior thanks Fundação de Amparo à Pesquisa do Estado de São Paulo (Brazil), Grant No. FAPESP# 2012/13179-6. Authors are grateful to the specialists of the characterization platform CMTC of Grenoble for careful measurements and discussion.

This work is dedicated to the memory of Prof Alain Reza Yavari, who was a mentor and insightful supervisor for some of the authors (DB, KG, NTP, AMJ).

REFERENCES

- [1] M. Dresselhaus, G. Crabtree, M. Buchanan, Eds, *Basic Energy Needs for the Hydrogen Economy*, Washington, DC, 2003.
- [2] *Targets for Onboard Hydrogen Storage Systems for Light-Duty Vehicles*, (2009) 5. http://www1.eere.energy.gov/hydrogenandfuelcells/storage/pdfs/targets_onboard_hydro_storage_explanation.pdf (accessed March 20, 2016).
- [3] M.E. Bluhm, M.G. Bradley, R. Butterick, U. Kusari, L.G. Sneddon, Amineborane-Based Chemical Hydrogen Storage: Enhanced Ammonia Borane Dehydrogenation in Ionic Liquids, *J. Am. Chem. Soc.* 128 (2006) 7748–7749. doi:10.1021/ja062085v.
- [4] F. Baitalow, J. Baumann, G. Wolf, K. Jaenicke-Rößler, G. Leitner, Thermal decomposition of B–N–H compounds investigated by using combined thermoanalytical methods, *Thermochim. Acta.* 391 (2002) 159–168. doi:10.1016/S0040-6031(02)00173-9.
- [5] C.A. Jaska, K. Temple, A.J. Lough, I. Manners, Transition Metal-Catalyzed Formation of Boron–Nitrogen Bonds: Catalytic Dehydrocoupling of Amine-Borane Adducts to Form Aminoboranes and Borazines, *J. Am. Chem. Soc.* 125 (2003) 9424–9434. doi:10.1021/ja030160l.
- [6] F.H. Stephens, R.T. Baker, M.H. Matus, D.J. Grant, D.A. Dixon, Acid Initiation of Ammonia–Borane Dehydrogenation for Hydrogen Storage, *Angew. Chemie Int. Ed.* 46 (2007) 746–749. doi:10.1002/anie.200603285.
- [7] M. Chandra, Q. Xu, A high-performance hydrogen generation system: Transition metal-catalyzed dissociation and hydrolysis of ammonia–borane, *J. Power Sources.* 156 (2006) 190–194. doi:10.1016/j.jpowsour.2005.05.043.
- [8] M. Chandra, Q. Xu, Room temperature hydrogen generation from aqueous ammonia–borane using noble metal nano-clusters as highly active catalysts, *J. Power Sources.* 168 (2007) 135–142. doi:10.1016/j.jpowsour.2007.03.015.
- [9] J. Hannauer, O. Akdim, U.B. Demirci, C. Geantet, J.-M. Herrmann, P. Miele, Q. Xu, High-extent dehydrogenation of hydrazine borane $N_2H_4BH_3$ by hydrolysis of BH_3 and decomposition of N_2H_4 , *Energy Environ. Sci.* 4 (2011) 3355. doi:10.1039/c1ee01886h.
- [10] J. Hannauer, U.B. Demirci, C. Geantet, J.-M. Herrmann, P. Miele, Transition metal-catalyzed dehydrogenation of hydrazine borane $N_2H_4BH_3$ via the hydrolysis of BH_3 and the decomposition of N_2H_4 , *Int. J. Hydrogen Energy.* 37 (2012) 10758–10767. doi:10.1016/j.ijhydene.2012.04.102.
- [11] A. Yousef, N.A.M. Barakat, M.H. EL-Newehy, M.M. Ahmed, H.Y. Kim, Catalytic hydrolysis of ammonia borane for hydrogen generation using Cu(o) nanoparticles supported on TiO_2 nanofibers, *Colloids Surfaces A Physicochem. Eng. Asp.* 470 (2015) 194–201. doi:10.1016/j.colsurfa.2015.02.004.
- [12] A. Zadick, L. Dubau, M. Chatenet, U. Demirci, A. Serov, P. Atanassov, Instability Of Commercial Pt/C And Pd/C Electrocatalysts In Alkaline Media, *ECS Trans.* 69 (2015) 553–558. doi:10.1149/06917.0553ecst.
- [13] A. Zadick, L. Dubau, N. Sergent, G. Berthomé, M. Chatenet, Huge Instability of Pt/C Catalysts in Alkaline Medium, *ACS Catal.* 5 (2015) 4819–4824. doi:10.1021/acscatal.5b01037.
- [14] A. Zadick, L. Dubau, U.B. Demirci, M. Chatenet, Effects of Pd Nanoparticle Size and Solution Reducer Strength on Pd/C Electrocatalyst Stability in Alkaline Electrolyte, *J. Electrochem. Soc.* 163 (2016) F781–F787. doi:10.1149/2.0141608jes.
- [15] L.C. Nagle, J.F. Rohan, Ammonia Borane Oxidation at Gold Microelectrodes in Alkaline Solutions, *J. Electrochem. Soc.* 153 (2006) C773. doi:10.1149/1.2344842.
- [16] E.H. Yu, X. Wang, U. Krewer, L. Li, K. Scott, Direct oxidation alkaline fuelcells: from materials to systems, *Energy Environ. Sci.* 5 (2012) 5668–5680. doi:10.1039/C2EE0252C.
- [17] J. Durst, A. Siebel, C. Simon, F. Hasché, J. Herranz, H.A. Gasteiger, New insights into the electrochemical hydrogen oxidation and evolution reaction mechanism, *Energy Environ. Sci.* 7 (2014) 2255. doi:10.1039/c4ee00440j.
- [18] P.-Y. Olu, F. Deschamps, G. Caldarella, M. Chatenet, N. Job, Investigation of platinum and palladium as potential anodic catalysts for direct borohydride and ammonia borane fuel cells, *J. Power Sources.* 297 (2015) 492–503. doi:10.1016/j.jpowsour.2015.08.022.
- [19] L.C. Nagle, J.F. Rohan, Nanoporous Gold Catalyst for Direct Ammonia Borane Fuel Cells, *J. Electrochem. Soc.* 158 (2011) B772. doi:10.1149/1.3583637.
- [20] M. Belén Molina Concha, M. Chatenet, F.H.B. Lima, E.A. Ticianelli, In situ Fourier transform infrared spectroscopy and on-line differential electrochemical mass spectrometry study of the NH_3BH_3 oxidation reaction on gold electrodes, *Electrochim. Acta.* 89 (2013) 607–615. doi:10.1016/j.electacta.2012.11.027.
- [21] X. Zhang, S. Han, J. Yan, H. Shioyama, N. Kuriyama, T. Kobayashi, Q. Xu, Electrochemical oxidation of ammonia borane on gold electrode, *Int. J. Hydrogen Energy.* 34 (2009) 174–179. doi:10.1016/j.ijhydene.2008.09.083.
- [22] K. Shimizu, A. Satsuma, Silver Cluster Catalysts for Green Organic Synthesis, *J. Japan Pet. Inst.* 54 (2011) 347–360. doi:10.1627/jpi.54.347.
- [23] T.A. Luft, www.strem.com, (n.d.). http://www.strem.com/uploads/technical_notes/47-0645tech.pdf (accessed February 7, 2016).
- [24] E. Detsi, M.S. Sellès, P.R. Onck, J.T.M. De Hosson, Nanoporous silver as electrochemical actuator, *Scr. Mater.* 69 (2013) 195–198. doi:10.1016/j.scriptamat.2013.04.003.
- [25] T. Spassov, L. Lyubenova, Y. Liu, S. Bliznakov, M. Spassova, N. Dimitrov, Mechanochemical synthesis, thermal stability and selective electrochemical dissolution of Cu–Ag solid solutions, *J. Alloys Compd.* 478 (2009) 232–236. doi:10.1016/j.jallcom.2008.12.005.
- [26] M. Chatenet, F. Micoud, I. Roche, E. Chainet, J. Vondrák, Kinetics of sodium borohydride direct oxidation and oxygen reduction in sodium hydroxide electrolyte, *Electrochim. Acta.* 51 (2006) 5452–5458. doi:10.1016/j.electacta.2006.02.014.
- [27] H. Cheng, K. Scott, Investigation of non-platinum cathode catalysts for direct borohydride fuel cells, *J. Electroanal. Chem.* 596 (2006) 117–123. doi:10.1016/j.jelechem.2006.07.031.
- [28] E. Sanli, H. Celikkan, B. Zuhtyuusal, M. Aksu, Anodic behavior of Ag metal electrode in direct borohydride fuel cells, *Int. J. Hydrogen Energy.* 31 (2006) 1920–1924. doi:10.1016/j.ijhydene.2006.04.003.
- [29] M.H. Atwan, D.O. Northwood, E.L. Gyenge, Evaluation of colloidal Ag and Ag-alloys as anode electrocatalysts for direct borohydride fuel cells, *Int. J. Hydrogen Energy.* 32 (2007) 3116–3125. doi:10.1016/j.ijhydene.2005.12.022.
- [30] E. Sanli, B.Z. Uysal, M.L. Aksu, The oxidation of $NaBH_4$ on electrochemically treated silver electrodes, *Int. J. Hydrogen Energy.* 33 (2008) 2097–2104. doi:10.1016/j.ijhydene.2008.01.049.
- [31] J. Erlebacher, M.J. Aziz, A. Karma, N. Dimitrov, K. Sieradzki, Evolution of nanoporosity in dealloying, *Nature.* 410 (2001) 450–453. doi:10.1038/35068529.
- [32] J. Erlebacher, An Atomistic Description of Dealloying, *J. Electrochem. Soc.* 151 (2004) C614. doi:10.1149/1.1784820.

- [33] J. Zhang, H. Ma, D. Zhang, P. Liu, F. Tian, Y. Ding, Electrocatalytic activity of bimetallic platinum-gold catalysts fabricated based on nanoporous gold, *Phys. Chem. Chem. Phys.* 10 (2008) 3250. doi:10.1039/b718192b.
- [34] M. Zhang, M.P. Li, T. Yin, T. Zhang, Fabrication of nanoporous bi-metallic Ag-Pd alloys with open pores, *Mater. Lett.* 162 (2016) 273-276. doi:10.1016/j.matlet.2015.10.014.
- [35] C. Xu, R. Wang, M. Chen, Y. Zhang, Y. Ding, Dealloying to nanoporous Au/Pt alloys and their structure sensitive electrocatalytic properties, *Phys. Chem. Chem. Phys.* 12 (2010) 239-246. doi:10.1039/B917788D.
- [36] C. Xu, L. Wang, X. Mu, Y. Ding, Nanoporous PtRu Alloys for Electrocatalysis, *Langmuir*. 26 (2010) 7437-7443. doi:10.1021/la9041474.
- [37] S. Van Petegem, S. Brandstetter, R. Maass, A.M. Hodge, B.S. El-Dasher, J. Biener, B. Schmitt, C. Borca, H. Van Swygenhoven, On the Microstructure of Nanoporous Gold: An X-ray Diffraction Study, *Nano Lett.* 9 (2009) 1158-1163. doi:10.1021/nl803799q.
- [38] J. Biener, G.W. Nye, A.M. Hodge, M.M. Biener, A. V. Hamza, S.A. Maier, Nanoporous Plasmonic Metamaterials, *Adv. Mater.* 20 (2008) 1211-1217. doi:10.1002/adma.200701899.
- [39] L. Liu, R. Scholz, E. Pippel, U. Gösele, Microstructure, electrocatalytic and sensing properties of nanoporous Pt₄₆Ni₅₄ alloy nanowires fabricated by mild dealloying, *J. Mater. Chem.* 20 (2010) 5621. doi:10.1039/c0jm00113a.
- [40] V. Zielasek, B. Jürgens, C. Schulz, J. Biener, M.M. Biener, A. V. Hamza, M. Bäumer, Gold Catalysts: Nanoporous Gold Foams, *Angew. Chemie Int. Ed.* 45 (2006) 8241-8244. doi:10.1002/anie.200602484.
- [41] A. Wittstock, B. Neumann, A. Schaefer, K. Dumbuya, C. Kübel, M.M. Biener, V. Zielasek, H.-P. Steinrück, J.M. Gottfried, J. Biener, A. Hamza, M. Bäumer, Nanoporous Au: An Unsupported Pure Gold Catalyst?, *J. Phys. Chem. C*. 113 (2009) 5593-5600. doi:10.1021/jp808185v.
- [42] M. Yan, Development of New Catalytic Performance of Nanoporous Metals for Organic Reactions, Springer Japan, 2014. doi:10.1007/978-4-431-54931-4.
- [43] D. Kramer, R.N. Viswanath, J. Weissmüller, Surface-Stress Induced Macroscopic Bending of Nanoporous Gold Cantilevers, *Nano Lett.* 4 (2004) 793-796. doi:10.1021/nl049927d.
- [44] J. Biener, a Wittstock, L. a Zepeda-Ruiz, M.M. Biener, V. Zielasek, D. Kramer, R.N. Viswanath, J. Weissmüller, M. Bäumer, a V Hamza, Surface-chemistry-driven actuation in nanoporous gold., *Nat. Mater.* 8 (2009) 47-51. doi:10.1038/nmat2335.
- [45] L.Y. Chen, J.S. Yu, T. Fujita, M.W. Chen, Nanoporous copper with tunable nanoporosity for SERS applications, *Adv. Funct. Mater.* 19 (2009) 1221-1226. doi:10.1002/adfm.200801239.
- [46] H. Qiu, Z. Zhang, X. Huang, Y. Qu, Dealloying Ag-Al Alloy to Prepare Nanoporous Silver as a Substrate for Surface-Enhanced Raman Scattering: Effects of Structural Evolution and Surface Modification, *ChemPhysChem*. 12 (2011) 2118-2123. doi:10.1002/cphc.201100205.
- [47] P. Ranga Reddy, K. Varaprasad, N. Narayana Reddy, K. Mohana Raju, N.S. Reddy, Fabrication of Au and Ag Bi-metallic nanocomposite for antimicrobial applications, *J. Appl. Polym. Sci.* 125 (2012) 1357-1362. doi:10.1002/app.35192.
- [48] L.Y. Chen, L. Zhang, T. Fujita, M.W. Chen, Surface-Enhanced Raman Scattering of Silver@Nanoporous Copper Core-Shell Composites Synthesized by an In Situ Sacrificial Template Approach, *J. Phys. Chem. C*. 113 (2009) 14195-14199. doi:10.1021/jp904081s.
- [49] T.N. Martin, Nanoporous and Thin Film Gold and Silver Metal Alloys and Their Medical Applications in Drug Delivery and Antimicrobial Activity, North Carolina State University, 2012.
- [50] A. Zalineeva, A. Serov, M. Padilla, U. Martinez, K. Artyushkova, S. Baranton, C. Coutanceau, P.B. Atanassov, Self-Supported Pd x Bi Catalysts for the Electrooxidation of Glycerol in Alkaline Media, *J. Am. Chem. Soc.* 136 (2014) 3937-3945. doi:10.1021/ja412429f.
- [51] A. Zalineeva, A. Serov, M. Padilla, U. Martinez, K. Artyushkova, S. Baranton, C. Coutanceau, P. Atanassov, Nano-structured Pd-Sn catalysts for alcohol electro-oxidation in alkaline medium, *Electrochem. Commun.* 57 (2015) 48-51. doi:10.1016/j.elecom.2015.05.006.
- [52] A. Zalineeva, A. Serov, M. Padilla, U. Martinez, K. Artyushkova, S. Baranton, C. Coutanceau, P.B. Atanassov, Glycerol electrooxidation on self-supported PdSn_x nanoparticles, *Appl. Catal. B Environ.* 176-177 (2015) 429-435. doi:10.1016/j.apcatb.2015.04.037.
- [53] C. Xu, Y. Li, F. Tian, Y. Ding, Dealloying to Nanoporous Silver and Its Implementation as a Template Material for Construction of Nanotubular Mesoporous Bimetallic Nanostructures, *ChemPhysChem*. 11 (2010) 3320-3328. doi:10.1002/cphc.201000313.
- [54] C. Xu, Y. Liu, F. Su, A. Liu, H. Qiu, Nanoporous PtAg and PtCu alloys with hollow ligaments for enhanced electrocatalysis and glucose biosensing, *Biosens. Bioelectron.* 27 (2011) 160-166. doi:10.1016/j.bios.2011.06.036.
- [55] Y. Jin, R. Li, T. Zhang, Formation of nanoporous silver by dealloying Ca-Ag metallic glasses in water, *Intermetallics*. 67 (2015) 166-170. doi:10.1016/j.intermet.2015.08.011.
- [56] M. Zhang, A.M. Jorge Junior, S.J. Pang, T. Zhang, A.R. Yavari, Fabrication of nanoporous silver with open pores, *Scr. Mater.* 100 (2015) 21-23. doi:10.1016/j.scriptamat.2014.11.040.
- [57] E. Detsi, Z. Vuković, S. Punzhin, P.M. Bronsveld, P.R. Onck, J.T.M. De Hosson, Fine-tuning the feature size of nanoporous silver, *CrystEngComm*. 14 (2012) 5402. doi:10.1039/c2ce25313e.
- [58] W.S. Rasband, <https://imagej.nih.gov/ij/>, U. S. Natl. Institutes Heal. Bethesda, Maryland, USA. (n.d.). <http://imagej.nih.gov/ij/> (accessed May 2, 2016).
- [59] N.L. Glinka, General Chemistry, KNORUS, Moscow, 2009.
- [60] P. Klobes, K. Meyer, R.G. Munro, Porosity and Specific Surface Area Measurements for Solid Materials, U.S. Government Printing Office, Washington, 2006. <http://www.ncbi.nlm.nih.gov/pubmed/22544181>.
- [61] U. Martinez, K. Asazawa, B. Halevi, A. Falase, B. Kiefer, A. Serov, M. Padilla, T. Olson, A. Datye, H. Tanaka, P. Atanassov, Aerosol-derived Ni_{1-x}Zn_x electrocatalysts for direct hydrazine fuel cells, *Phys. Chem. Chem. Phys.* 14 (2012) 5512. doi:10.1039/c2cp40546f.
- [62] A. Serov, U. Martinez, A. Falase, P. Atanassov, Highly active PdCu catalysts for electrooxidation of 2-propanol, *Electrochem. Commun.* 22 (2012) 193-196. doi:10.1016/j.elecom.2012.06.023.
- [63] T. Sakamoto, K. Asazawa, U. Martinez, B. Halevi, T. Suzuki, S. Arai, D. Matsumura, Y. Nishihata, P. Atanassov, H. Tanaka, Electrooxidation of hydrazine hydrate using Ni-La catalyst for anion exchange membrane fuel cells, *J. Power Sources*. 234 (2013) 252-259. doi:10.1016/j.jpowsour.2013.01.181.
- [64] A. Serov, U. Martinez, P. Atanassov, Novel Pd-In catalysts for alcohols electrooxidation in alkaline media, *Electrochem. Commun.* 34 (2013) 185-188. doi:10.1016/j.elecom.2013.06.003.
- [65] T. Sakamoto, K. Asazawa, J. Sanabria-Chinchilla, U.

- Martinez, B. Halevi, P. Atanassov, P. Strasser, H. Tanaka, Combinatorial discovery of Ni-based binary and ternary catalysts for hydrazine electrooxidation for use in anion exchange membrane fuel cells, *J. Power Sources*. 247 (2014) 605–611. doi:10.1016/j.jpowsour.2013.08.107.
- [66] Micromeritics 2011, ASAP 2020 Accelerated Surface Area and Porosimetry System Operator's Manual, V4.01, (n.d.). http://www.cif.iastate.edu/sites/default/files/uploads/Other_Inst/BET/ASAP2020_Operator's_Manual.pdf (accessed February 10, 2016).
- [67] M. Pourbaix, *Atlas d'équilibres électrochimiques*, Gauthier-V, 1963.
- [68] L.C. Nagle, J.F. Rohan, Nanoporous gold anode catalyst for direct borohydride fuel cell, *Int. J. Hydrogen Energy*. 36 (2011) 10319–10326. doi:10.1016/j.ijhydene.2010.09.077.
- [69] P.-Y. Olu, C.R. Barros, N. Job, M. Chatenet, Electrooxidation of NaBH_4 in Alkaline Medium on Well-defined Pt Nanoparticles Deposited onto Flat Glassy Carbon Substrate: Evaluation of the Effects of Pt Nanoparticle Size, Inter-Particle Distance, and Loading, *Electrocatalysis*. 5 (2014) 288–300. doi:10.1007/s12678-014-0195-0.
- [70] D.A. Finkelstein, C.D. Letcher, D.J. Jones, L.M. Sandberg, D.J. Watts, H.D. Abruña, Self-Poisoning during BH_4^- Oxidation at Pt and Au, and in Situ Poison Removal Procedures for BH_4^- Fuel Cells, *J. Phys. Chem. C*. 117 (2013) 1571–1581. doi:10.1021/jp308677f.

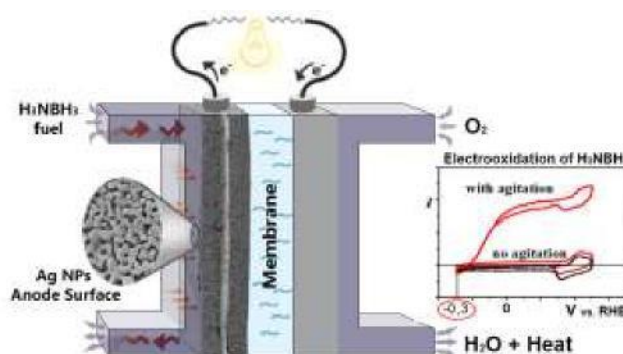


Table of Contents